J|A|C|S ARTICLES

Published on Web 02/02/2010

Nature of N−N Bonding within High-Pressure Noble-Metal Pernitrides and the Prediction of Lanthanum Pernitride

Michael Wessel and Richard Dronskowski*

Institute of Inorganic Chemistry, RWTH Aachen University, Landoltweg 1, 52056 Aachen, Germany

Received December 15, 2009; E-mail: drons@HAL9000.ac.rwth-aachen.de

Abstract: The nature of nitrogen−nitrogen bonding and the metal oxidation states within late-noble-metal pernitrides have been determined by a series of density-functional electronic-structure calculations. In contrast to alkaline-earth pernitrides such as BaN_2 which contain quasi-molecular double-bonded N_2^{2-} units, compounds such as PtN_2 incorporate a tetravalent metal and a N_2^{4-} species with a N−N single bond due to four surplus electrons within the antibonding $1\pi_g^*$ molecular orbital. This fact is the source of the huge bulk moduli of PtN_2 and related materials such as OsN_2 and IrN_2. The crystal structure of lanthanum pernitride, $LaN_2 \rightleftarrows La^{3+} + N_2^{2-} + e^-$, yet to be made, has been predicted, and its electronic structure is compared with a likewise hypothetical LaN_2 which consists of both N_2^{2-} and N_2^{4-} pernitride units together with a trivalent lanthanum cation. Finite-temperature DFT calculations predict a very moderate reaction pressure toward LaN_2 starting from LaN and elemental nitrogen of less than 2 GPa at 300 K.

1. Introduction

Within the realm of nitrogen-rich solid-state materials, extended compounds such as barium pernitride, BaN_2,[1] and strontium pernitride, SrN_2,[2] were the first to be synthesized and structurally characterized in 2001. In addition, AN_2 compounds, with A being an element from main group IV, were theoretically investigated in 2003,[3,4] but it was not until the discovery of platinum pernitride, PtN_2,[5] that such materials found significant interest outside solid-state chemistry, namely, in the field of material science. The discovery of PtN_2 is a fascinating story by itself because this particular phase was erroneously characterized in terms of both chemical composition ("PtN") and also structure (zinc blende) at the very beginning. Independent theoretical[6] and experimental[7] research later showed that PtN does *not* exist and that PtN_2—the correct composition—adopts the pyrite [FeS_2] type. Even today, PtN_2 is still incorrectly formulated as a "nitride" here and there despite the fact that nitride phases contain, by definition, isolated nitrogen anions with a formal anionic charge of −3, which would yield an implausible oxidation state of +6 for the platinum atom. PtN_2, however, contains nitrogen *dimers*; thus, it must be called platinum pernitride or diazenide. Likewise, hydrogen peroxide (but not water) is the correct term for H_2O_2.

Because of the above-mentioned interest in pernitride chemistry, the past five years have witnessed the syntheses or theoretical predictions of other fascinating noble-metal pernitrides such as IrN_2,[7] OsN_2,[8] and, most recently, PdN_2.[9] All these pernitrides have been reported as mechanically hard materials, and their hardnesses exceed those of the noble metals. Thus, it is obvious from the outset that the existence of the nitrogen dimers is the physicochemical source of the large hardnesses, but where does it originate from, exactly?

Figure 1 offers a view into the crystal structures of BaN_2, PtN_2, OsN_2, and IrN_2. The N−N distances in the noble-metal pernitrides are 1.41 Å for PtN_2, 1.43 Å for OsN_2, and 1.42 Å for IrN_2 such that the bond-length similarity points toward a related bonding scheme. If we take the archetypal phase platinum pernitride, for example, a plausible formulation would be "$Pt^{2+}N_2^{2-}$", just like for the alkaline-earth phase BaN_2 for which the charge balance $Ba^{2+}N_2^{2-}$ clearly holds. In the phase BaN_2, however, the N−N distance is significantly shorter, namely, 1.23 Å. Alternatively, the formulation "$Pt^{4+}N_2^{4-}$" might better reflect the true bonding scenario. It is the aim of this paper to clarify the above question of N−N chemical bonding and the Pt oxidation state in PtN_2 and the role of N−N bonding in other high-pressure pernitrides and to predict a new interesting synthetic target on the basis of this chemical understanding.

2. Theoretical Methods

The *ab initio* calculations were based on the plane-wave pseudopotential strategy by means of the computer program VASP (Vienna *Ab Initio* Simulation Package)[10,11] using the generalized

(1) Vajenine, G. V.; Auffermann, G.; Prots, Y.; Schnelle, W.; Kremer, R. K.; Simon, A.; Kniep, R. *Inorg. Chem.* **2001**, *40*, 4866.
(2) Auffermann, G.; Prots, Y.; Kniep, R. *Angew. Chem., Int. Ed.* **2001**, *40*, 547.
(3) Weihrich, R.; Matar, S. F.; Betranhandy, E.; Eyert, V. *Solid State Sci.* **2003**, *5*, 701.
(4) Weihrich, R.; Eyert, V.; Matar, S. F. *Chem. Phys. Lett.* **2003**, *373*, 636.
(5) Gregoryanz, E.; Sanloup, C.; Somayazulu, M.; Badro, J.; Fiquet, G.; Mao, H.-K.; Hemely, R. J. *Nat. Mater.* **2004**, *3*, 294.
(6) von Appen, J.; Lumey, M.-W.; Dronskowski, R. *Angew. Chem., Int. Ed.* **2006**, *45*, 4365.
(7) Crowhurst, J. C.; Goncharov, A. F.; Sadigh, B.; Evans, C. L.; Morrall, P. G.; Ferreira, J. L.; Nelson, A. J. *Science* **2006**, *311*, 1275.
(8) Montoya, J. A.; Hernandez, A. D.; Sanloup, C.; Gregoryanz, E.; Scandolo, S. *Appl. Phys. Lett.* **2007**, *90*, 011909.
(9) Crowhurst, J. C.; Goncharov, A. F.; Sadigh, B.; Zaug, J. M.; Aberg, D.; Meng, Y.; Prakapenka, V. B. *Nat. Mater.* **2008**, *23*, 294.
(10) Kresse, G.; Furthmüller, J. *Comput. Mater. Sci.* **1996**, *6*, 15. Kresse, G.; Furthmüller, J. *Phys. Rev. B* **1996**, *55*, 11169.

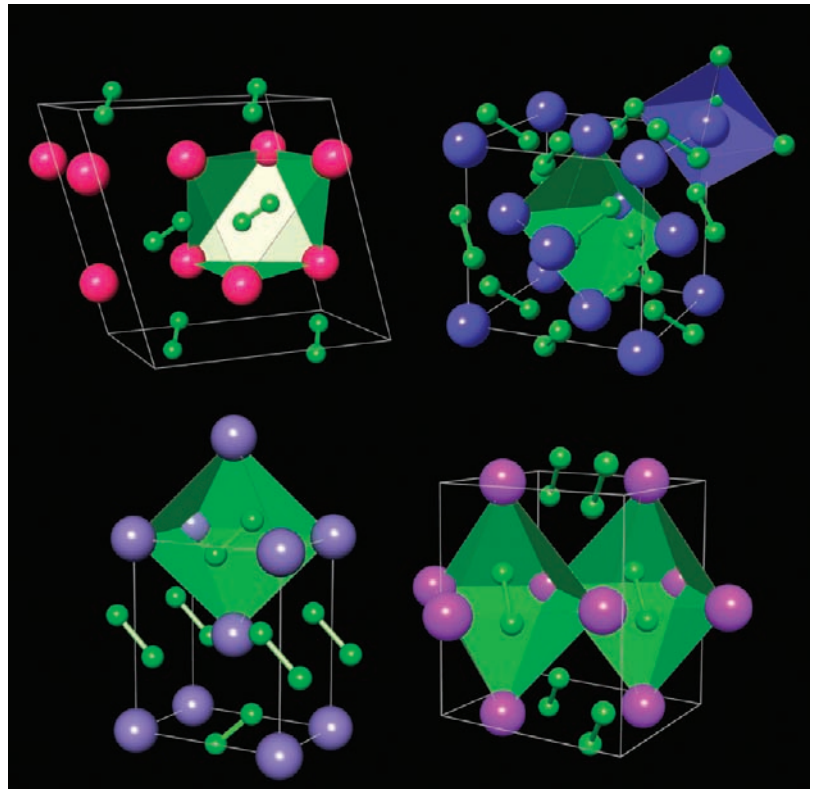

Figure 1. Crystal structures of BaN_2 (top left), PtN_2 (top right), OsN_2 (bottom left), and IrN_2 (bottom right) in which the (green) pernitride dimers and the surrounding coordination polyhedra have been highlighted.

gradient approximation (GGA) of PBE type[12] and the projector-augmented wave (PAW) method.[13] A cutoff energy of 500 eV was chosen, and a dense net of at least 300 *k* points per cell was used. The structures of the noble-metal pernitrides and the alkaline-earth pernitrides were taken from the literature, their unit cells were allowed to change in volume and shape, and all atomic positions were also allowed to relax. For the composition LaN_2, a set of 29 commonly known AB_2 structures was used as a starting point to find the structures lying lowest in energy, and the electronic-structure calculations proceeded as before. After having arrived at the optimized unit cells, their volumes were changed around the ambient-pressure equilibrium value (91−105%) and bulk moduli were obtained by fitting Murnaghan-type equations of state to the calculated energy−volume data. In addition, two more LaN_2 structures were constructed by hand by alluding to the fascinating high-pressure crystal chemistry of strontium.[2] Starting from a hexagonal close-packed La lattice, a scenario corresponding to $La^{3+} + (N{=}N)^{2-} + e^-$ and another one with a bonding idea of $La^{3+} + {}^1/_2(N{=}N)^{2-} + {}^1/_2(N{-}N)^{4-}$ were also computationally studied, in the first case using a spin-polarized and in the second one using a spin-restricted approach. Whenever needed, chemical bonding analyses were carried out by means of the crystal orbital Hamilton population (COHP) method[14] implemented in the all-electron quasi-relativistic TB-LMTO-ASA[15] program package. Theoretical phonon data were calculated using the quasi-harmonic approximation by means of the FROPHO utility[16] together with VASP, and thermodynamical state functions were then generated using a set of script programs[17] on the basis of the density-functional electronic structure. Structural drawings were performed using Balls & Sticks.[18]

3. Results and Discussion

To understand N−N bonding and the metal oxidation state in PtN_2, one needs to answer the question of whether $Pt^{2+}N_2^{2-}$ or $Pt^{4+}N_2^{4-}$ is the more appropriate charge calculus, and this may be done by looking at either Pt or N. We will first concentrate on nitrogen−nitrogen bonding. Thus, Figure 2 offers the canonical molecular-orbital diagram of the nitrogen molecule, N_2, in the valence region but with three different electron counts.

For the neutral N_2 molecule, the $2\sigma_g$ and $1\pi_u$ molecular orbitals are filled with six electrons to result in an exceedingly strong N≡N triple bond with a bond distance of 1.10 Å and a huge dissociation enthalpy of 946 kJ/mol, making the N_2 molecule an extremely inert species. Adding two more electrons into the antibonding $1\pi_g^*$ molecular orbitals yields the species N_2^{2-}, which is isoelectronic with molecular oxygen; the latter paramagnetic molecule is characterized by a longer O═O double bond of 1.21 Å and a smaller dissociation enthalpy of 498 kJ/mol. Note that the reduction of the bonding multiplicity is simply due to the two surplus electrons sitting in the antibonding $1\pi_g^*$ orbitals. By adding another two electrons into these orbitals, we arrive at N_2^{4-}, which is isoelectronic with the fluorine

(11) Kresse, G.; Hafner, J. *Phys. Rev. B* **1993**, *47*, 558. Kresse, G.; Hafner, J. *Phys. Rev. B* **1994**, *49*, 14251.
(12) Perdew, J. P.; Burke, K.; Ernzerhof, M. *Phys. Rev. Lett.* **1996**, *77*, 3865.
(13) Blöchl, P. E. *Phys. Rev. B* **1994**, *50*, 17953.
(14) Dronskowski, R.; Blöchl, P. E. *J. Phys. Chem.* **1993**, *97*, 8617.
(15) Tank, R. Jepsen, O. Burkhardt, A. Andersen., O. K. *LMTO*, version 4.7; MPI für Festkörperforschung: Stuttgart, Germany, 2000.
(16) Togo, A. *FROPHO: A Tool To Compute Phonon Band Structures and Thermal Properties of Solids*; RWTH Aachen University: Aachen, Germany, 2007/2008; available at http://fropho.sourceforge.net. Togo, A.; Oba, F.; Tanaka, I. *Phys. Rev. B* **2008**, *78*, 13410.
(17) Stoffel, R. Doctoral Dissertation, RWTH Aachen University, Aachen, Germany, in preparation.
(18) Ozawa, T. C.; Kang, S. J. *J. Appl. Crystallogr.* **2004**, *37*, 679.

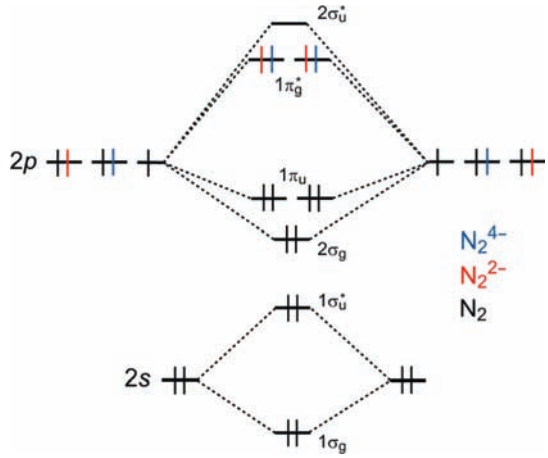

Figure 2. Qualitative molecular-orbital diagram of the N_2 molecule with three different degrees of electron filling in the valence region.

molecule, which has a much wider F−F single bond of 1.42 Å and an even smaller dissociation enthalpy of only 159 kJ/mol.

Judging from the N−N distances, the N_2 unit in PtN_2[19] (1.41 Å) almost perfectly matches the F−F distance and the single-bond scenario, rather than being similar to the O═O double bond with 1.21 Å. The latter, however, clearly relates to the N_2 unit in BaN_2 (1.23 Å). Thus, we tentatively conclude that $Pt^{4+}N_2^{4-}$ is the correct electron count despite the existence of $Ba^{2+}N_2^{2-}$. This analysis is in perfect agreement with earlier experimental work[20] in which the N−N bond in PtN_2 was directly studied by Raman spectroscopy and where the vibrational modes of PtN_2 were calculated using density-functional perturbation theory. Both the experimental and theoretical spectra show frequency shifts which had also been observed for single-bonded nitrogen in the polymeric cg N-phase.[21] This phase is a high-pressure and high-temperature polymorph of nitrogen found above 110 GPa and 2000 K. Nonetheless, we note that such comparisons are somewhat problematic because the peaks do shift as a function of external pressure. For example, the nitrogen single-bond peak in the aforementioned cg N-phase is predicted at 780 cm^{-1} for zero pressure while it is found at 840 cm^{-1} for 115 GPa.

Another indirect way to subject to proof the Pt^{2+} oxidation state is given by Raman spectroscopy as recently suggested by Vajenine.[22] If we look at the Raman spectrum of a solid-state material incorporating double-bonded nitrogen dimers, such as diimide (N_2H_2), the characteristic frequency for the −N═N− linkage is located at 1550 cm^{-1}.[23] Unfortunately, the experimental Raman spectrum of BaN_2 is unknown, but the theoretical calculations yield a value of 1466 cm^{-1}. The corresponding density-functional calculations for the late-noble-metal pernitrides, however, result in characteristic peaks for the N−N single-bond vibration at much lower values, namely, 752 cm^{-1} for PtN_2, 836 cm^{-1} for IrN_2,[24] and 778 cm^{-1} for OsN_2;[25] see also Table 1.

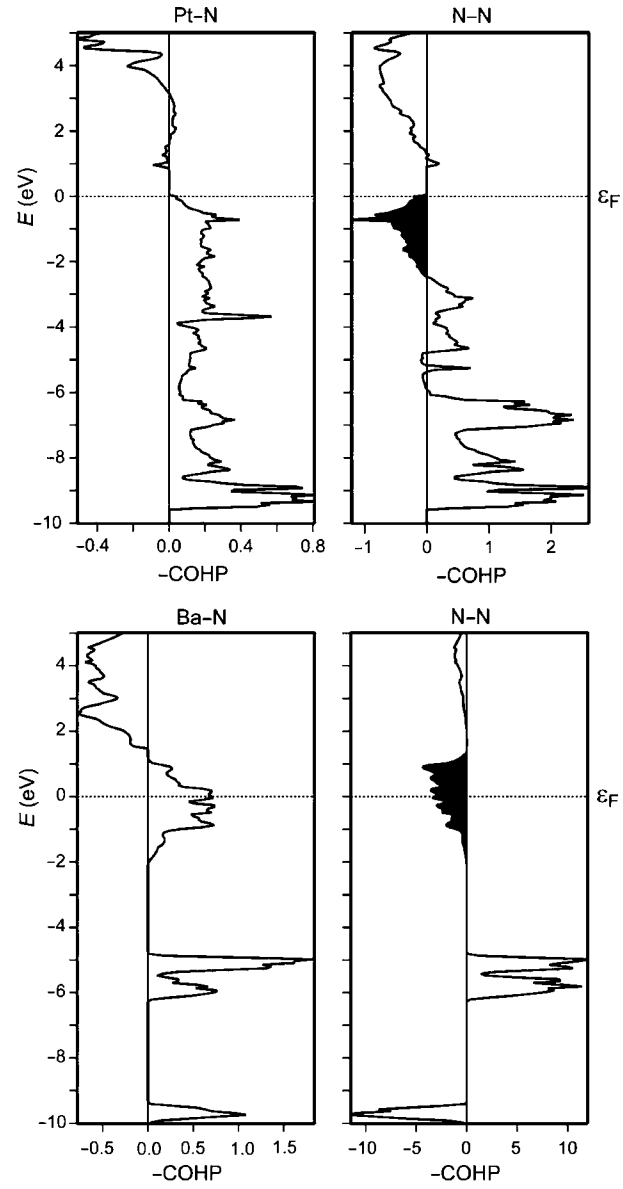

Figure 3. COHP analysis of Pt−N and N−N bonding within PtN_2 (top) and Ba−N and N−N bonding within BaN_2 (bottom).

Table 1. Selected Structural and Physical Properties of Various Metal Pernitrides

	SrN_2	BaN_2	LaN_2	OsN_2	IrN_2	PtN_2
N−N distance (Å)	1.25	1.23	1.30	1.42	1.43	1.41
characteristic Raman frequency (cm^{-1})		1466		752	778	836
B_0 (GPa)	65	46	86			256[6]

If we stick to the $Pt^{4+}N_2^{4-}$ description for the moment, a quantum-chemical analysis of the extended structure of PtN_2 indeed yields the antibonding states within the quasi-molecular nitrogen dimer mentioned above. Figure 3 (top) offers the

(19) Relaxed structural parameters for PtN_2: $Pa\bar{3}$ (No. 205), a = 4.810 Å, Pt on 4a, N on 8c with x = 0.415, N−N = 1.41 Å.
(20) Young, A. F.; Montoya, J. A.; Sanloup, C.; Lazzeri, M.; Gregoryanz, E.; Scandolo, S. *Phys. Rev. B* **2006**, *73*, 153102.
(21) Eremets, M. I.; Gavriliuk, A.; Trojan, I.; Dzivenko, D.; Boehler, R. *Nat. Mater.* **2004**, *3*, 558.
(22) Vajenine, G. V. Nitride der Alkali-, Erdalkali-und Übergangsmetalle. Habilitationsschrift, Technische Universität Stuttgart, Stuttgart, Germany, 2009.
(23) Bondybey, V. E.; Nibler, J. W. *J. Phys. Chem.* **1973**, *58*, 2125.
(24) Relaxed structural parameters for IrN_2: $P2_1/c$ (No. 14), a = 4.879 Å, b = 4.933 Å, c = 4.918 Å, β = 107.95°, Ir on 4e with x = 0.233, y = 0, and z = 0.221, N(1) on 4e with x = 0.325, y = 0.414, and z = 0.160, N(2) on 4e with x = 0.186, y = 0.597, and z = 0.299, N−N = 1.43 Å.
(25) Relaxed structural parameters for OsN_2: *Pnnm* (No. 58), a = 4.142 Å, b = 4.953 Å, c = 2.696 Å, Os on 2a, N on 4g with x = 0.126 and y = 0.403, N−N = 1.42 Å.

COHPs for the Pt−N and the N−N bonding inside PtN_2, and it also shows those of the Ba−N and the N−N bonding inside BaN_2 (bottom). In all plots, bonding states are given as spikes to the right whereas antibonding states show up as spikes to the left. For the Pt−N combination, there are only bonding states in the entire occupied region, and antibonding states show up in the unoccupied crystal orbitals, well above the Fermi level (dotted horizontal zero line). For the N−N combination in PtN_2, however, the antibonding $1\pi_g$* states are clearly seen (in black) between ca. −2.5 eV and the Fermi level. When investigating the Ba−N interaction, we also find bonding states up to 1 eV in BaN_2, but the N−N interaction differs from that in PtN_2. Here, the antibonding states are found between −2 and +2 eV, but they are only filled by 50%. Since the huge hardness of PtN_2 goes back to these completely filled antibonding states, we may predict that BaN_2 and SrN_2, with only two electrons in the $1\pi_g$* states, will exhibit much smaller hardnesses. Because no experimental data were found for BaN_2 and SrN_2, we calculated their theoretical bulk moduli from first principles. The obtained values for BaN_2 (B_0 = 46 GPa) and SrN_2 (B_0 = 65 GPa) are indeed much smaller than that of PtN_2 (B_0 = 256 GPa),[6] thereby semiquantitatively supporting the above argument.

We now consider the same problem but focus on the local geometrical and electronic structure of the platinum atom. With respect to the electron count of Pt, the formulation of $Pt^{2+}N_2^{2-}$ refers to a d^8 configuration whereas $Pt^{4+}N_2^{4-}$ is equivalent to a d^6 scenario for platinum. Here, a look at the crystal structure of PtN_2 (Figure 1) is helpful because Pt exhibits octahedral coordination by nitrogen such that the ligand-field splitting follows the e_g above t_{2g} scheme, with all six electrons buried in the low-lying t_{2g} set. For a d^8 electron count, however, the two surplus electrons would go into the higher lying e_g set.

Fortunately enough, there are other platinum compounds for comparison, and these do not pose any difficulties for the determination of the oxidation states. On purpose, we choose chlorine compounds of platinum because Cl exhibits the same Pauling electronegativity (3.0) as N. Thus, Figure 4 (top) displays the crystal structure of the well-established phase K_2PtCl_6 in which platinum also exhibits octahedral coordination by chlorine, and the charge calculus simply reads $(K^+)_2$-$Pt^{4+}(Cl^-)_6$, i.e., tetravalent platinum. Alternatively, $PtCl_2$, with an electron count of $Pt^{2+}(Cl^-)_2$, is given in Figure 4 (bottom), and here the d^8 configuration is reflected by the square-planar coordination of Pt by Cl; the leftover electrons are used by platinum to engage in platinum−platinum multicenter bonding inside a Pt_6 octahedron.

Not too surprisingly, the structural similarity of PtN_2 with K_2PtCl_6 but not with $PtCl_2$, indicative of a d^6 (Pt^{4+}) but not d^8 (Pt^{2+}) electron configuration, is also mirrored in the theoretical densities of states, visualized in Figure 5. For PtN_2, a band gap clearly separates the occupied t_{2g} from the unoccupied e_g set such that Pt^{4+} is the correct oxidation state. For this Pt^{4+}, the ratio of the integrated occupied and unoccupied d states is 3.1:1.9, which is very close to the expected 3:2 ratio. A similar behavior is found for K_2PtCl_6 with respect to the roles of the t_{2g} and e_g sets; note, however, that the larger ionic character of the chemical bonding in K_2PtCl_6 leads to a less dispersive density of states (DOS). For K_2PtCl_6, we find a ratio of 3.3:1.7 for the d states, which is still close the 3:2 ratio, thereby suggesting Pt^{4+}.

For the case of $PtCl_2$, however, the situation changes qualitatively because two more electrons have entered the occupied region below the Fermi level. Taking into account the different (square-planar) ligand field of Pt in $PtCl_2$, the t_{2g} below e_g scenario of point group O_h changes into an $(e_g + b_{2g}) + a_{1g}$ below b_{1g} case for D_{4h}, which, for d orbitals, translates into four occupied orbitals, d_{xz}, d_{yz}, d_{xy}, and d_{z^2}, and one unoccupied orbital, $d_{x^2-y^2}$. This is exactly what is depicted in Figure 5, with the unoccupied $d_{x^2-y^2}$ orbital located around 1 eV above the Fermi level. The integrated ratio of the occupied and unoccupied d states is 4.1:0.9, extremely close the ideal 4:1 ratio and corroborating the platinum d^8 configuration.

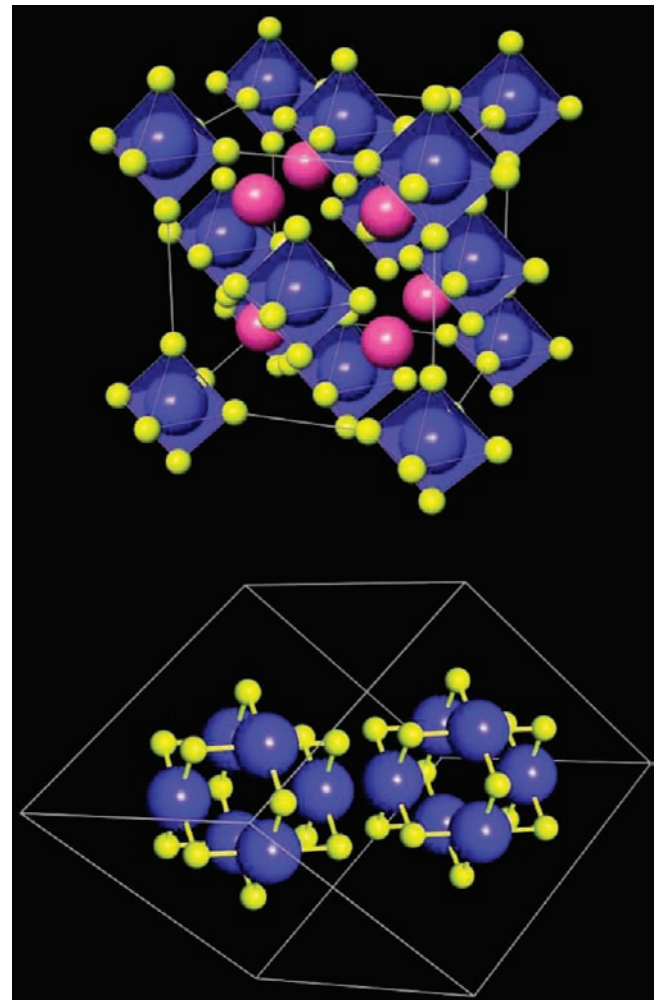

Figure 4. Crystal structures of K_2PtCl_6 (top) and $PtCl_2$ (bottom) with K in pink, Pt in blue, and Cl in yellow.

To conclude, bond-length considerations and spectroscopic results in combination with molecular-orbital arguments clearly support a single-bonded $(N-N)^{4-}$ unit in PtN_2; only the latter anionic charge, that is, four surplus electrons within antibonding $1\pi_g$* states, allows us to understand its spectroscopic properties and also its huge bulk modulus. Likewise, the oxidation state of Pt is a clear +4 because of the structural similarity with K_2PtCl_6 (and not $PtCl_2$), and this argument is fully supported by the theoretical densities of states.

What about the other transition-metal pernitrides such as OsN_2 and IrN_2? As mentioned earlier, all of them exhibit octahedral metal coordination and similar N−N distances around 1.4 Å such that a charge balance of N_2^{4-} in all those cases is a very good working hypothesis. As seen before, the theoretical densities of states as shown in Figure 6 are helpful in this respect. On the right we find the DOS of the already discussed PtN_2. Because iridium is platinum's left neighbor in the periodic

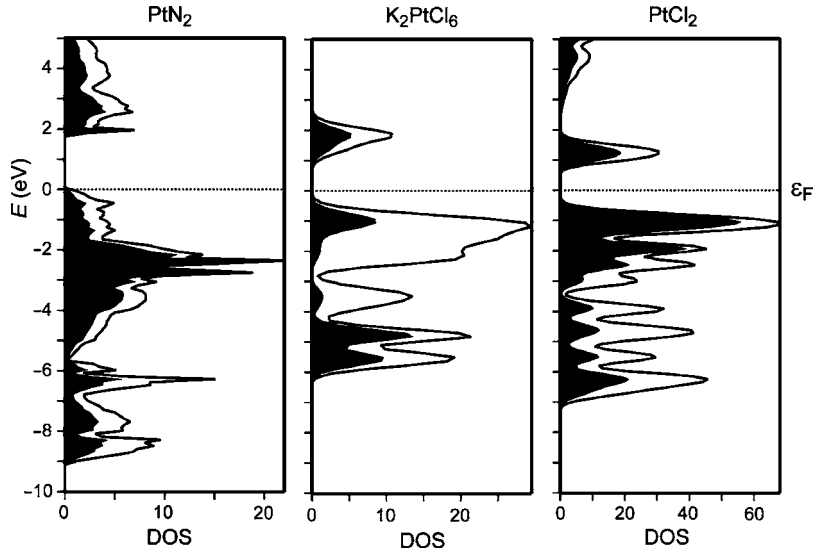

Figure 5. Total and d-projected (in black) DOS for PtN_2 (left), K_2PtCl_6 (middle), and $PtCl_2$ (right).

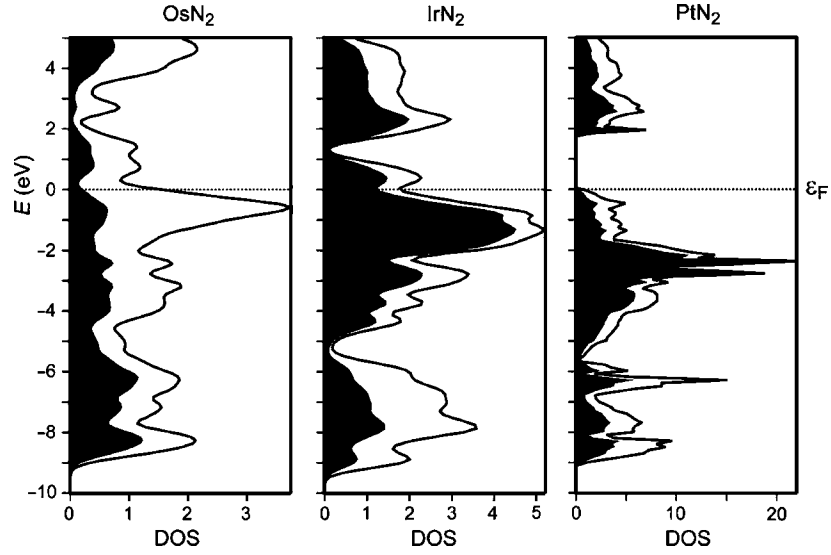

Figure 6. Same as Figure 5, but for OsN_2 (left), IrN_2 (middle), and PtN_2 (right).

table and has one fewer electron, we plot the DOS of IrN_2 left of that of PtN_2 in the middle of Figure 6. By assuming an Ir^{4+} oxidation state and a d^5 configuration, the t_{2g} band contains one hole such that a metallic character would be predicted for IrN_2, without any calculation. This prediction is clearly fulfilled because the t_{2g} set is filled by five-sixths. Above the t_{2g} hole, at ca. 1.2 eV, one finds the band gap beyond which the likewise unoccupied e_g bands are located.

The case of OsN_2 is slightly more difficult. Assuming a +4 oxidation for osmium yields a d^4 configuration for the t_{2g} set. Although Jahn−Teller distortions are very unlikely to result from partially filled t_{2g} sets, the real structure of OsN_2 does exhibit such (small) distortion because the OsN_6 octahedron is slightly distorted to result in a quadratic bipyramid (D_{4h}) with two shorter (Os−N1 = 2.06 Å) and four slightly longer (Os−N2 = 2.11 Å) bonds. In principle, the former t_{2g} set splits into a fully occupied e_g (d_{xz}, d_{yz}) and an empty b_{2g} (d_{xy}). Because of the tiny bond-length difference, the two sets of bands can hardly be resolved from the DOS of OsN_2 (Figure 6, left). Nonetheless, it is obvious that two-thirds of the former t_{2g} set is occupied such that $Os^{4+}N_2^{4-}$ is the correct formulation of osmium pernitride.

The above investigation on the charge of pernitride units and the corresponding oxidation states of the metal ions suggests additional interesting questions: What will happen for a pernitride incorporating a *trivalent* instead of di- and tetravalent transition metal? Is the presence of N_2^{4-} or N_2^{2-} units thinkable, and how can the charge balance be reached? To answer these questions, lanthanum was used as the metal of choice. No experimental structure data for the composition LaN_2 are known from the literature, such that 31 different possible AB_2 structures were computationally studied. After total optimization, the final energy−volume results are given in Table 2 and displayed in Figure 7.

The structural ground state of LaN_2 is best described by a slightly distorted [ThC_2] structure type (Tables 3 and 4). For this structure, depicted in the upper part of Figure 8, one finds a hexagonal close-packing of lanthanum atoms in which the pernitride units occupy the octahedral voids. As is evident from

Table 2. Total Energies and Molar Volumes for Hypothetical Lanthanum Pernitride, LaN_2, in 31 Different Structure Types

structure type	*E* (kJ/mol)	*V* (cm^3/mol)	structure type	*E* (kJ/mol)	*V* (cm^3/mol)
Al_2Cu	−2217.5	25.84	Ga_2Sr	−2234.7	24.45
AlB_2	−2095.8	23.54	hcp 2	−2248.7	29.85
CaC_2 (ht)	−2329.2	26.13	hcp 2 + 4	−2111.4	26.73
CaC_2 (rt)	−2330.8	27.49	HgI_2	−1985.7	31.15
CaF_2	−1928.3	28.36	La_2Sb	−1998.7	26.19
CaI_2	−2104.1	23.61	MgC_2	−2345.0	28.12
CaI_2 (hp)	−2094.8	31.01	NbS_2	−2182.6	37.35
$CdCl_2$	−2110.0	23.80	$PbCl_2$	−2124.7	25.50
Co_2Si	−2121.4	25.57	PbClF	−1996.3	26.10
Cu_2Mg	−1795.9	22.81	$SiSr_2$	−1871.9	24.69
Cu_2S	−2333.2	26.32	**ThC_2**	**−2348.6**	**26.76**
$CuZr_2$	−2325.4	25.75	TiO_2 (badd)	−2289.9	35.69
dist FeS_2	−2309.9	28.24	TiO_2 (rutile)	−1845.4	34.16
dist MgC_2	−2248.3	30.11	$ZnCl_2$	−2039.7	41.28
FeS_2 (ht)	−2209.3	27.03	ZrO_2	−2322.2	25.94
FeS_2 (rt)	−2309.6	28.23			

Table 5, LaN_2 is an exothermic phase (−11 kJ/mol at absolute zero temperature) compared to the simple 1:1 nitride LaN and elemental nitrogen, and it also has a smaller volume by −6.6 cm^3/mol. We therefore predict this compound to be stable under standard conditions once it has been synthesized, in particular by applying moderate pressure (see below) at not too high temperatures, similar to the case of BaN_2.[1] For this medium-pressure LaN_2 phase, the calculated bulk module ($B_0 = 86$ GPa) is slightly larger than those of the alkaline-earth pernitrides but considerably lower than those of the transition-metal pernitrides. The N−N interatomic distance points into a similar direction: it is 1.30 Å for LaN_2, which is slightly larger than those for BaN_2 (1.23 Å) and SrN_2 (1.25 Å) but clearly shorter than that for PtN_2 (1.41 Å). Since La *cannot* exist as La^{4+} and since there is only one N_2 unit present, the idea of a N_2^{2-} unit is at hand, in particular because LaN_2 has metallic properties (see below). This idea can be nicely studied with another computational

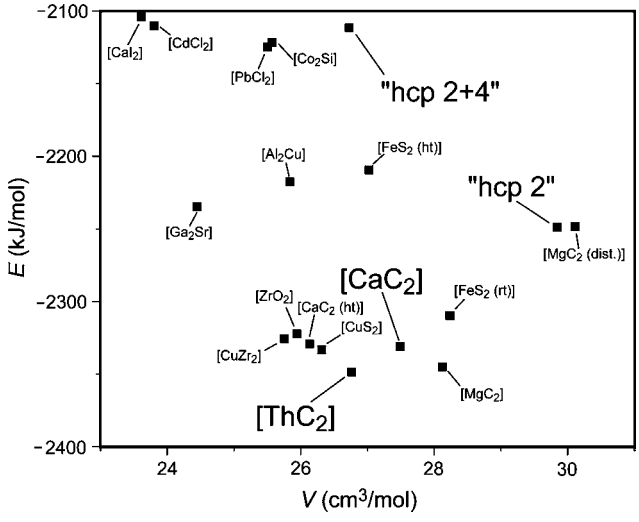

Figure 7. Density-functional energy−volume diagram for various structural alternatives of the composition LaN_2; also see the text.

Table 3. Theoretically Predicted Space Groups and Lattice Parameters for Three Hypothetical Crystal Structures of Lanthanum Pernitride

structure type	space group	*a* (Å)	*b* (Å)	*c* (Å)	*β* (deg)
ThC_2	*C*2/*c*	6.759	4.138	6.528	103.19
hcp 2	*P*31*m*	6.566	=*a*	7.966	
hcp 2 + 4	*P*31*m*	6.214	=*a*	7.963	

Table 4. Theoretically Predicted Spatial Parameters for Three Hypothetical Crystal Structures of Lanthanum Pernitride

structure type	atom	Wyckoff position	*x*	*y*	*z*
ThC_2	La	8f	0.0	0.785	3/4
	N	4e	0.699	0.867	0.947
hcp 2	La(1)	6d	2/3	0.0	0.4793
	La(2)	6d	2/3	2/3	0.907
	N(1)	1a	0.0	0.0	0.1473
	N(2)	1a	0.0	0.0	0.3127
	N(3)	1a	0.0	0.0	0.6475
	N(4)	1a	0.0	0.0	0.8125
	N(5)	2b	1/3	2/3	0.1473
	N(6)	2b	1/3	2/3	0.3127
	N(7)	2b	1/3	2/3	0.6475
	N(8)	2b	1/3	2/3	0.8125
hcp 2 + 4	La(1)	6d	0.6722	0.0	0.46
	La(2)	6d	0.3278	0.0	0.0
	N(1)	1a	0.0	0.0	0.15
	N(2)	1a	0.0	0.0	0.31
	N(3)	1a	0.0	0.0	0.64
	N(4)	1a	0.0	0.0	0.82
	N(5)	2b	1/3	2/3	0.15
	N(6)	2b	1/3	2/3	0.31
	N(7)	2b	1/3	2/3	0.64
	N(8)	2b	1/3	2/3	0.82

model, one for which we probe the +3 oxidation state of La in combination with the pernitride unit's potential to disproportionate for reasons of charge balance.

To do so, one needs to compare a model system that might be formulated as (i) $La^{3+} + N_2^{2-} + e^-$ with another one that would be called (ii) $La^{3+} + {}^1/_2N_2^{2-} + {}^1/_2N_2^{4-}$; note that a similar anionic disproportionation (but with N^{3-} and N_2^{2-}) is responsible for the existence of SrN.[2] The two corresponding crystal structures—i and ii—are easily generated from a modified $[Fe_3N]$ type but with a composition of La_6N_{12} because then the octahedral voids of a closed-packed lanthanum lattice are filled with pernitride units. For establishing model ii, 50% of the pernitride units were given a starting N−N distance of 1.23 Å while the remaining pernitride units were set to a 1.40 Å bond length; we will call this the "hcp 2 + 4" model of LaN_2. The earlier model i with only one N_2^{2-} unit and a N−N distance of 1.23 Å is naturally called "hcp 2". Figure 8 (bottom) displays these structural ideas. Upon optimizing both models, it turns out that hcp 2 + 4 can *only* be stabilized by a spin-restricted description against changing into hcp 2 because spin polarization removes the activation barrier of charge transfer between the pernitride units. Table 4 also has the spatial parameters after structural optimization in which the N−N distance is 1.31 Å

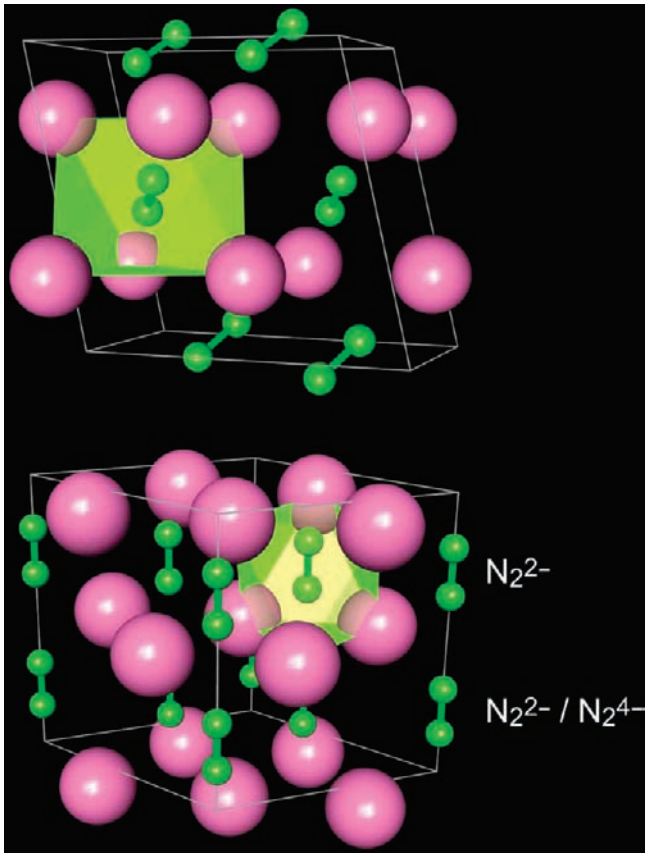

Figure 8. Predicted crystal structure of LaN_2 in the $[ThC_2]$ structure type (top) and in two other structures incorporating the hexagonal close-packed motif (bottom). In the latter, LaN_2 may solely contain N_2^{2-} dimers but also a 1:1 mixture of N_2^{2-} and N_2^{4-} pernitride units; also see the text.

Table 5. Relative Theoretical Formation Enthalpies, Molar Volumes, and Bulk Modules B_0 and Their Derivatives B_0' (at V_0) of LaN_2 in Different Structures Compared to LaN and Elemental N_2

	ΔH (kJ/mol)	ΔV (cm³/mol)	B_0 (GPa)	B_0'	N−N distance (Å)
$LaN + {}^1/_2\alpha\text{-}N_2$	0.0	0.00			
LaN_2 $[ThC_2]$	−11.0	−6.60	86	5.26	1.30
LaN_2 [hcp 2]	88.0	−3.52			1.31
LaN_2 [hcp 2 + 4]	225.3	−6.64			1.27/1.43

for hcp 2 while it is 1.27 and 1.43 Å for hcp 2 + 4, close to our simple guess at the very beginning.

The energy difference between hcp 2 + 4 and hcp 2 is astonishingly large, and the structure solely containing the N_2^{2-} pernitride unit is clearly lying much lower in energy, by 137 kJ/mol (Table 5), such that the idea of pernitride disproportionation must be discarded; on the contrary, hcp 2 is much closer to the $[ThC_2]$ ground state. The electronic differences between hcp 2 + 4 and hcp 2 are obvious from the DOS shown in Figure 9. Besides common features such as the filled N 2s states (between −11 and −9 eV), the hcp 2 model has the bonding π states of the $(N{=}N)^{2-}$ unit located between −7 and −4 eV (in red) while for the hcp 2 + 4 model the π states of the $(N{=}N)^{4-}$ unit (−7 to −5 eV, blue) are separated from the higher lying states of the $(N{=}N)^{2-}$ unit (−5 to −3 eV, red). All π^* states of the dinitrogen units lie in the proximity of the Fermi level, between −2 and +3 eV, together with the lanthanum 5d and also 4f orbitals. Here, the nonvanishing DOS points toward metallic phases, and the additional delocalized charge density mixing into the π^* states of the N−N units

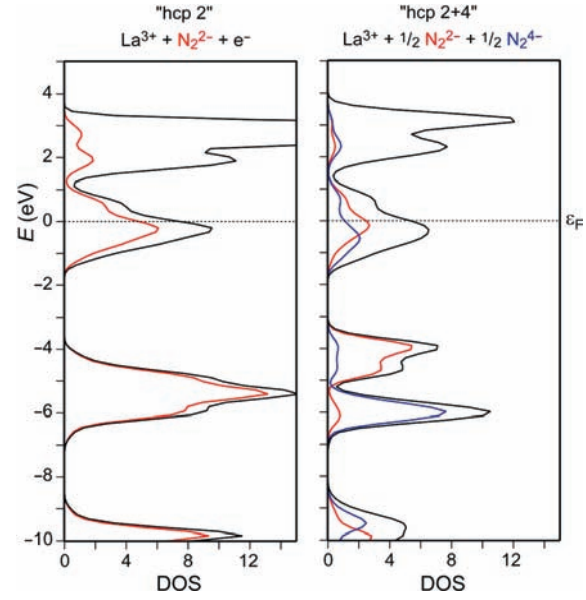

Figure 9. Density of states diagrams for LaN_2 with hexagonally close-packed La atoms and N_2^{2-} pernitride units (left) and a 1:1 mixture of N_2^{2-} and N_2^{4-} pernitride units (right) in the octahedral sites. The contributions of the complex anions have been highlighted in red (N_2^{2-}) and blue (N_2^{4-}).

suggests that their electron count must be slightly higher than the formal one. Indeed, the final interatomic distance of $(N{=}N)^{2-}$ unit in both models is 1.27 and 1.31 Å, larger than the expected 1.23 Å.

Let us compare the electronic structure for the predicted LaN_2 adopting the $[ThC_2]$ type with those of similar well-known compounds. Figure 10 (far left) offers the total and C-projected (in black) DOS for barium acetylide, BaC_2.[26] As expected, the virtual Ba 6s levels have been emptied to completely fill the π valence band arising from the acetylide unit below (between −4 and −1 eV) to result in the electronic formulation $Ba^{2+} + (C{\equiv}C)^{2-}$ and insulating behavior. By adding one additional electron for the case of the isostructural phase LaC_2,[27] the π states (Figure 10, left) become much more diffuse and are now located between −5 and −2 eV. Instead of localizing the 5d electron on the La atoms, their 5d orbitals hybridize with the acetylide π states (between −1 and +2 eV) and lead to a finite DOS at the Fermi level. This further introduction of additional charge density is mirrored by the fact that the diazenide unit is elongated, with an interatomic distance of 1.30 Å, slightly larger than the undisturbed C≡C triple bond (1.27 Å) in insulating BaC_2. Thus, $La^{3+} + (C{\equiv}C)^{2-} + e^-$ is the proper formulation.

If we replace the $(C{\equiv}C)^{2-}$ unit by the $(N{=}N)^{2-}$ unit, we arrive at a hypothetical LaN_2 crystallizing in the $[CaC_2]$ type. The additional two electrons allow the bonding π states to move down to an energy region between −7 and −4 eV (Figure 10, right). Above that, we find three different valence states, with lanthanum 5d being the most diffuse (between −2 and +2.5 eV) one. It mixes mostly with the π^* states (between −1 and +1 eV) of the $(N{=}N)^{2-}$ unit and also, to a lesser extent, with the virtual lanthanum 4f states (between 2 and 3 eV). The N=N distance of 1.30 Å for the $[CaC_2]$ type is identical with that of LaN_2 in the lowest lying $[ThC_2]$ type. The additional structural change of LaN_2 from the $[CaC_2]$ type to

(26) Vohn, V.; Kockelmann, W.; Ruschewitz, U. *J. Alloys Compd.* **1999**, *284*, 132.
(27) Stackelberg, M. v. *Z. Phys. Chem.* **1930**, *B9*, 437.

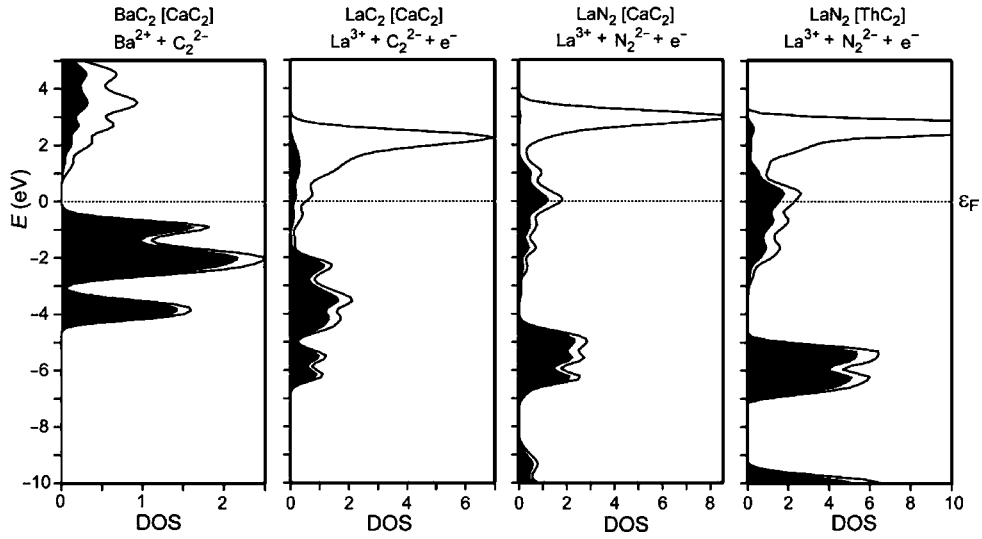

Figure 10. Total and C/N-projected (in black) DOS diagrams for BaC_2 in the $[CaC_2]$ type, LaC_2 in the $[CaC_2]$ type, LaN_2 in the $[CaC_2]$ type, and LaN_2 in the $[ThC_2]$ type.

the $[ThC_2]$ type only leads to minute changes in the electronic structure (Figure 10, far right), and this is also reflected by the small energy difference of only 18 kJ/mol between the two. Both are metallic and best described by an electron count that goes as $La^{3+} + (N{=}N)^{2-} + e^-$.

Eventually, we will cover the synthetic conditions under which the synthesis of LaN_2 in the $[ThC_2]$ structure type should be accomplished. While Table 5 shows that LaN_2 is predicted as being exothermic by −11 kJ/mol with respect to LaN and elemental nitrogen, this numerical value for the formation enthalpy according to the reaction

$$LaN + {}^1/_2\alpha\text{-}N_2 \rightarrow LaN_2$$

only refers to absolute zero temperature and *solid* nitrogen. Since we plan to synthesize LaN_2 at room temperature or close to that, however, the lattice vibrations of the solid phases LaN_2 and LaN and solid N_2 must be taken into account, as well as the $T\Delta S$ term for the gaseous nitrogen molecule, to go from absolute zero enthalpies toward Gibbs energies. Formally, the gibbs formation energy of LaN_2 at a temperature of 300 K reads as follows:

$$\begin{aligned}\Delta G_f^{300} &= G^{300}(LaN_2) - G^{300}(LaN) - {}^1/_2 G^{300}(N_2) \\ &= G^{300}(LaN_2) - G^{300}(LaN) - {}^1/_2[H^{300}(N_2) - \\ &\qquad 300\ K \cdot \Delta S^{300}(N_2)]\end{aligned}$$

While the experimental formation enthalpy of nitrogen is zero by definition, we note that the DFT calculation is based on the total electronic energy U at absolute zero temperature such that we may write

$$H^{300}(N_2) = U(N_2) + \int_0^{300} C_p(N_2,T)\,dT \approx U(N_2) + C_p{}^{300}(N_2) \times 300\ K$$

thereby having approximated the heat capacity of nitrogen. This eventually gives

$$\Delta G_f^{300} = G^{300}(LaN_2) - G^{300}(LaN) - {}^1/_2 U(N_2) - {}^1/_2 C_p{}^{300}(N_2) \times 300\ K + {}^1/_2 \Delta S^{300}(N_2) \times 300\ K$$

for the free formation energy of LaN_2. The corresponding density-functional phonon calculations and thermochemical integrations yield that the Gibbs energy of the product LaN_2 is lowered by ca. −15 kJ/mol upon going from $T = 0$ K to room temperature while that of the educt LaN is lowered even more, by ca. −20 kJ/mol; at room temperature this would make the reaction less likely by +5 kJ/mol compared to absolute zero temperature.

Because nitrogen is gaseous at 300 K, the Gibbs free energy includes three more entries. With respect to the total electronic energy, there is no change compared to that at absolute zero temperature. The heat capacity term $C_p\Delta T$[28] lowers the Gibbs free energy by 9 kJ/mol (in this case ca. 4 kJ because we deal with half a molecule), but there is the expected destabilization of LaN_2 by the large entropic term $T\Delta S$ of 58 kJ/mol[28] (here 29 kJ for half a nitrogen molecule). As a result, ΔG arrives at +22 kJ/mol for the reaction. Since this reaction is endergonic, it will be nonspontaneous.

To make the reaction still proceed, pressure must be used, as is depicted in Figure 11. The pressure-dependent Gibbs free energies of LaN and LaN_2 were also determined by performing phonon calculations, while the Gibbs free energy of nitrogen under pressure and at a temperature of 300 K was classically estimated in the same manner as in the previous paragraph. We confess that this is accompanied by a small error because at moderate pressures (up to 2 GPa) and at 300 K[29] nitrogen already turns liquid. Thus, the entropy of nitrogen is *overestimated* so that the fifth term of the above equation for the Gibbs reaction energy is too large. As a result, the true value of ΔG_f^{300} will be more negative and the formation will take place at lower pressures than estimated. If we define the horizontal line as the total Gibbs energies of the starting materials, the dotted line then represents G of the target phase LaN_2. The sketch clearly indicates that the synthesis of LaN_2 should be tried at room temperature and a very moderate pressure of less than 2 GPa because beyond that pressure the Gibbs energy of LaN_2 is predicted to be lower than those of LaN and elemental nitrogen.

(28) *D'Ans-Lax Taschenbuch für Chemiker und Physiker*, 4th ed.; Blachnik, R., Ed.; Springer Verlag: Berlin, Heidelberg, Germany, 1998; Vol. III.
(29) Bini, R.; Ulivi, L.; Kreutz, J.; Jodl, H. J. *J. Chem. Phys.* **2000**, *112*, 8522.

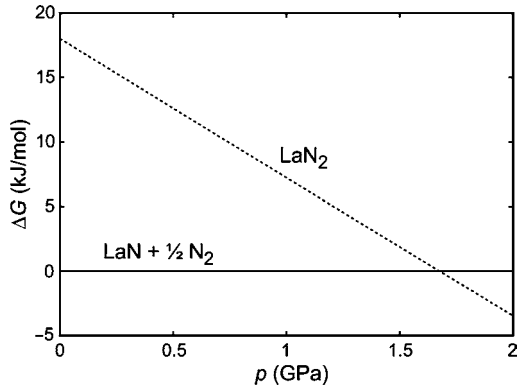

Figure 11. Density-functional Gibbs free energy−pressure diagram for the synthesis of LaN_2 in the [ThC_2] type at a projected synthetic temperature of $T = 300$ K; also see the text.

Kinetic reasons may require slightly higher temperatures and, therefore, slightly larger reaction pressures.

4. Conclusion

The nature of N−N bonding and the oxidation state of the late-noble-metal pernitrides OsN_2, IrN_2, and PtN_2 have been studied from ab initio calculations of density-functional (PAW-GGA-PBE) type. The conclusions are based on theoretical densities of states, calculated Raman frequencies, mechanical hardnesses, and local structural characteristics such as coordination numbers and N−N distances. The obtained data unambiguously show that all late-noble-metal pernitrides contain tetravalent metal atoms in combination with a N_2^{4-} pernitride unit, irrespective of the metallic nature of OsN_2 and IrN_2, in obvious contrast to the alkaline-earth pernitrides which consist of M^{2+} ions together with N_2^{2-} pernitride units. In addition, the existence of the hypothetical, yet-to-be-synthesized phase lanthanum pernitride, LaN_2, has been suggested. This metallic compound is likely to crystallize in the [ThC_2] type, a high-pressure phase predicted as being exothermic with respect to LaN and elemental nitrogen at absolute zero temperature. Its electron count is best described as $La^{3+} + N_2^{2-} + e^-$, similar to the already known phase LaC_2 crystallizing in the [CaC_2] type. On the basis of finite-temperature phonon calculations and empirical thermochemical data for molecular nitrogen, we furthermore predict LaN_2 to form at room temperature already at a moderate pressure of less than 2 GPa.

Acknowledgment. We thank the Deutsche Forschungsgemeinschaft (DFG) for financial support and the computing center of RWTH Aachen University for providing us with their supercomputing facilities.

JA910570T